Liquid Crystals
Publication details, including instructions for authors and subscription information:
http://www.informaworld.com/smpp/title~content=t713926090

Computer simulations of nematic droplets

Axel Kilian[a]
[a] Institut fur Theoretische Physik, Technische Universität Berlin, Berlin 12, Germany

To cite this Article Kilian, Axel(1993) 'Computer simulations of nematic droplets', Liquid Crystals, 14: 4, 1189 — 1198
To link to this Article: DOI: 10.1080/02678299308027827
URL: http://dx.doi.org/10.1080/02678299308027827

LIQUID CRYSTALS, 1993, VOL. 14, NO. 4, 1189–1198

Computer simulations of nematic droplets

by AXEL KILIAN
Institut für Theoretische Physik, Technische Universität Berlin,
D-1000 Berlin 12, Germany

Nematic droplets are intimately connected with disclinations, because in nematic droplets, point and line-shaped defects, as well as surface defects, are not generated at random, but inevitably by topological constraints. Thus, droplets provide a good means for investigating nematic defects. There is a growing interest in both topics due to the applications in polymer dispersed liquid crystal devices [1–3], but also in classical display modelling, where nematic defects are to be avoided. Various types of droplets are investigated theoretically with the aid of a previously developed numerical algorithm [4, 5], which is based on a dynamic equation for the alignment tensor $a_{\mu\nu}$. The rotational diffusion, the influence of an orienting external field, and the Frank elasticity (in the one-coefficient approximation) are taken into account, but flow processes are neglected. For the application to nematic droplets, a new type of boundary conditions had to be used, which I have called 'true planar anchoring'. I simulate the relaxation of the director field of nematic droplets from the isotropic state and vice versa for various types of anchoring and cavity shapes. Contrast pictures, as if viewed under crossed Nicols, are computed and compared to experiment. The results obtained elucidate the nature of the surface disclinations of strength one (boojums). In particular, it is found that their occurrence can be understood as a consequence of the planar anchoring, without any further assumptions. Moreover, a phase transition-like transformation of the director configuration is predicted which is temperature controlled and occurs, as the blue phases do, close to the nematic–isotropic transition temperature T_c.

1. Introduction

This paper proceeds as follows: in § 2, some basic facts about nematic droplets are reviewed. In § 3, the basic equations for the dynamics of the nematic alignment tensor are introduced, and two numerical algorithms with different degrees of specialization are derived: the simpler one is formulated in terms of the nematic director, whereas the more sophisticated one contains the Landau–De Gennes potential and can therefore simulate the nematic–isotropic transition. Both methods are capable of handling nematic defects (disclinations). In § 4, which is the main part of this paper, computer simulations of nematic droplets are presented and discussed. The last section is devoted to the conclusions and acknowledgments.

2. Nematic droplets reviewed

Nematic droplets may be characterized by a number of features, for example, the droplet size, the cavity shape, the type of surface alignment induced by the respective interfacial material, the material constants (K_1, K_2, K_3, γ_1), the sign of the dielectric anisotropy $\Delta\varepsilon$, to name some of them. They all contribute to the complex behaviour observed in experiments. Since this is a theoretical paper, we will focus on the director configuration, which is not directly measurable but governs the electro-optical response and the phase contrast.

0267-8292/93 $10·00

As a first approximation, Doane *et al.* [1] classify the droplets by their surface alignment, which may be either planar, or homeotropic. This leads to four basic types of director fields within the droplets: the planar droplets usually exhibit a bipolar alignment, that is, a strongly aligned director field with two surface disclinations of strength 1 (boojums) at the antipodal points of the bipolar axis (see figure 1 (*a*)). If, however, the ratio of the bend to splay constants, K_{33}/K_{11} is less than unity, concentric (toroidal) structure (see figure 1 (*b*)) can appear. That director configuration was identified by Drzaic [6]. For homeotropically aligned droplets there are also two different director configurations, the radial and the axial configuration (see figure 2). The radial configuration is spherically symmetric, whereas the axial one has cylindrical symmetry. As was found theoretically and in accordance with experiment, there is a critical droplet radius $R_c = 18{\cdot}2\,K_{11}/W_0$, below which the axial configuration is energetically preferred due to the scaling laws of wall and bulk energies [7]. The authors speak of a configuration transition controlled by the droplet size, which may be misleading because for a given droplet the size is fixed. Another similar configuration transition was found by Lavrentovich and Terentjev [8], which is in contrast driven by the ratio K_{11}/K_{33}, and could therefore be observed experimentally, using the divergence of K_{33} at the smectic transition temperature.

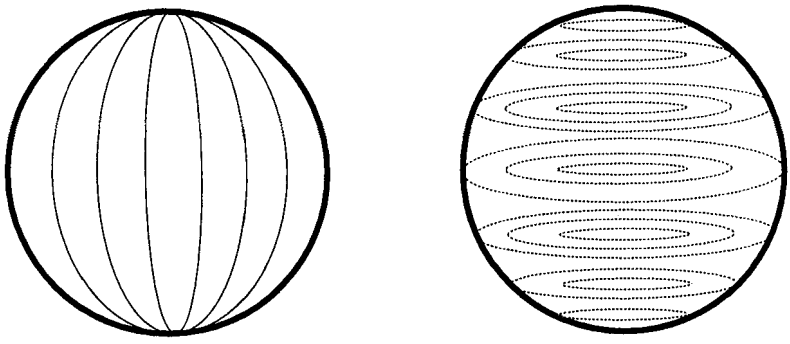

(*a*) (*b*)

Figure 1. (*a*) Bipolar and (*b*) toroidal director configuration of droplets with planar surface alignment.

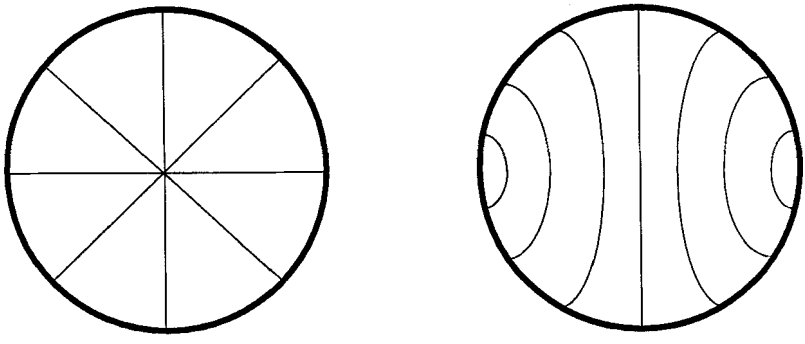

(*a*) (*b*)

Figure 2. (*a*) Radial and (*b*) axial director configuration of droplets with homeotropic surface alignment.

2.1. *Theory*

2.1.1. *Basic equations*

The orientation of (effectively) uniaxial molecules with their figure axis parallel to the unit vector **u** is characterized by the (second rank) alignment tensor

$$a_{\mu\nu} = \langle \overline{u_\mu u_\nu} \rangle. \tag{1}$$

The brackets $\langle\ \rangle$ indicate an average (to be evaluated with the one-particle distribution function), and the bar refers to the symmetric-traceless (irreducible) part of the tensor. I assume the following nonlinear relaxation equation for **a** [9]:

$$\tau_a \frac{\partial a_{\mu\nu}}{\partial t} + \xi_0^2 \nabla^2 a_{\mu\nu} + \Phi_{\mu\nu}(\mathbf{a}) - F_{\mu\nu}(\mathbf{a}) = 0. \tag{2}$$

The first term is a damping term; the second term describes the Frank elasticity in the one-coefficient approximation, i.e. $K_{11} = K_{22} = K_{33}$. The quantity $\Phi_{\mu\nu}$ is a generalized force represented by the derivatives of a (dimensionless) Landau–De Gennes potential, and $F_{\mu\nu}$ describes the influence of an external orienting field. The phenomenological coefficients ξ_0 and τ_a are related to the Frank elastic constant according to

$$K = 3a_{\text{eq}}^2 \xi_0^2 \frac{\rho}{m} k_B T; \tag{3a}$$

$$\gamma_1 = 3a_{\text{eq}}^2 \tau_a \frac{\rho}{m} k_B T. \tag{3b}$$

Further details may be found in [1]. This equation allows a unified treatment of non-equilibrium phenomena in the isotropic and the nematic phases, including the pretransitional phenomena. To simplify equation (2), I will assume uniaxiality, i.e.

$$a_{\mu\nu} = a\sqrt{\tfrac{3}{2}}\, \overline{n_\mu n_\nu}. \tag{4}$$

This approximation is supported by a recently performed linear stability analysis of the Landau–De Gennes potential, which revealed that the uniaxial state is stable [10].

2.1.2. *Simple algorithm*

At constant temperature one can assume

$$a = a_{\text{eq}} = S\sqrt{5}, \tag{5}$$

where $S = \langle P_2(n_\mu u_\mu) \rangle$ is the Maier–Saupe order parameter. The assumption that the scalar order parameter is constant holds not strictly, but turned out to be a good approximation, for the following reason: the correlation length ξ_0 in equation (2) is of molecular size (for example 5 Å for MBBA, *cf.* equation (3 *a*)). As a consequence, the disclination size is of the same order of magnitude, which means that the decay of the scalar order parameter from its equilibrium value to zero inside the disclination core takes place within a distance of one molecular length. The physical meaning of this statement is obscure; moreover, it clearly leaves the range of validity of equation (2), which is based on a mezzo-scale theory (that is, one volume element is large enough to contain as many molecules as needed to yield reasonable expectation values.† Thus,

† More reliable predictions of the decay of the scalar order parameter inside a disclination core have been obtained from molecular theories, for example Zannonis Monte-Carlo simulations, *cf.* [13].

equation (5) holds for any macroscopic length scale. The corresponding constraint can be imposed on equation (2) by an exterior product, i.e.

$$\varepsilon_{\lambda\kappa\mu}a_{\kappa\nu}\left(\tau_a\frac{\partial a_{\mu\nu}}{\partial t}-\xi_0^2\nabla a_{\mu\nu}-F_{\mu\nu}\right)=0. \tag{6}$$

Note that $\alpha_{\mu\nu}$ now has the form given by equations (4) and (5); $\varepsilon_{\lambda\kappa\mu}$ is the totally antisymmetric tensor of rank 3. Equation (6) is first discretized on a uniform mesh, and thereafter multiplied by n_ν. This results in the following numerical algorithm for a constant scalar order parameter:

$$n_\mu^{\text{new}}=\lambda[\overline{(n_\mu n_\nu}+\beta\hat{E}_\mu\hat{E}_\nu)n_\nu], \tag{7}$$

The parameter λ has to be calculated at every lattice point such that $n_\mu n_\mu=1$; γ_1 is the rotational viscosity, δl the mesh size, and K the Frank elastic constant. The maximum numerically-stable time step $\delta t=\gamma_1\delta l^2/(6K)$ was chosen. The field strength E determines $\beta=\varepsilon_0\varepsilon_a\delta l^2E^2/(6K)$. If not stated otherwise, algorithm (7) has been used throughout this paper.

2.1.3. *Enhanced algorithm*

If one wants to simulate the nematic–isotropic phase transition, the Landau–De Gennes potential can no longer be neglected. I have developed an extended numerical algorithm where the alignment is still uniaxial, but the scalar order parameter a is free. This leads to the expression of an 'alignment vector' $N_\mu=an_\mu$. Its dynamics is given by

$$\tau_a\frac{\partial}{\partial t}N_\mu-\xi_0^2n_\nu\Delta(N_\mu n_\nu)+\frac{2}{3}(A(T)-a+a^2)N_\mu-a^{-1}F_{\mu\nu}n_\nu=0. \tag{8}$$

In order to get rid of the material parameters B and C occurring in the Landau–De Gennes potential, all quantities in this equation have been scaled in units of combinations of B and C, the temperature-independent coefficients of the Landau–De Gennes potential. They should therefore be distinguished from the previously defined quantities by a suitable tag, which I sacrifice for brevity. The remaining parameter $A(T)$ controls the temperature. Setting it to zero corresponds to $T=T^*$, which is sometimes called the pseudo-critical temperature (below T^*, no metastable isotropic phase is possible); the clearing point is at $A_c=2/9$, and above $A^+=1/4$, the isotropic phase is stable, i.e. no metastable nematic phase is possible.

Discretizing equation (8) leads to the following numerical algorithm for the alignment vector (the term $F_{\mu\nu}$ is omitted, because phase transitions in the presence of an external field have so far not been simulated):

$$N_\mu^{\text{new}}=\left(1-\frac{2\delta t}{3\tau_a}(A-a+a^2)\right)N_\mu+\frac{\delta t}{\tau_a}\frac{\xi_0^2}{\delta x^2}\sum_{i=1}^{6}(N_\mu^i s^i-N_\mu). \tag{9}$$

Again, δx and δt are the mesh size and the time step, respectively.

2.1.4. *Representation of the director field*

Due to the huge amount of data, it is not possible to represent the entire simulated director field. A sample is taken, which is done by selecting the sites with the highest anisotropic energy. In this way, the presentation resembles those pictures usually seen under the polarization microscope, because the locations with high anisotropic energy

yield at the same time a high phase contrast for polarized light. It will be referred to as 'defect representation'. The defect representation shows only the vicinity of the disclinations and therefore enables the examination of the disclination type.

2.1.5. *Representation of the mean alignment*

As a piece of additional information, the mean alignment of the droplet is represented as a rectangular box located in the droplet centre which represents $\langle n_\mu n_\nu \rangle$. For small droplets (in the range of 400 μm or less) a similar averaging occurs by visible light passing through the droplets, so that this mean alignment, which is in general not uniaxial, provides information about the anisotropy of the effective dielectic permittivity tensor.

2.1.6. *Boundary conditions*

For homeotropically aligned droplets, rigid anchoring was assumed. However, this is not suitable for planar anchoring on a sphere. Instead, a new type of boundary condition was modelled, which will be referred to as true planar anchoring. It means that the director (or the alignment vector, equivalently) can freely rotate within the local tangent plane of the droplet.

2.1.7. *Phase contrast pictures*

The phase contrast pictures depicted below have been calculated according to the Mueller matrix formalism [11]. That is, the phase shift of monochromatic light passing through the droplet is calculated for every grid point (assuming the light passes in a prescribed direction), but diffraction is not taken into account.

3. Simulations

3.1. *Homeotropically aligned droplets*

In this simulation, the simple algorithm for a fixed scalar order parameter was used. In order to achieve a solution which is not biased by any assumptions, I start from a quasi-isotropic state consisting of randomly distributed directors. The result was an axial director configuration (see figure 3 (*a*)), accompanied by the usual disclination

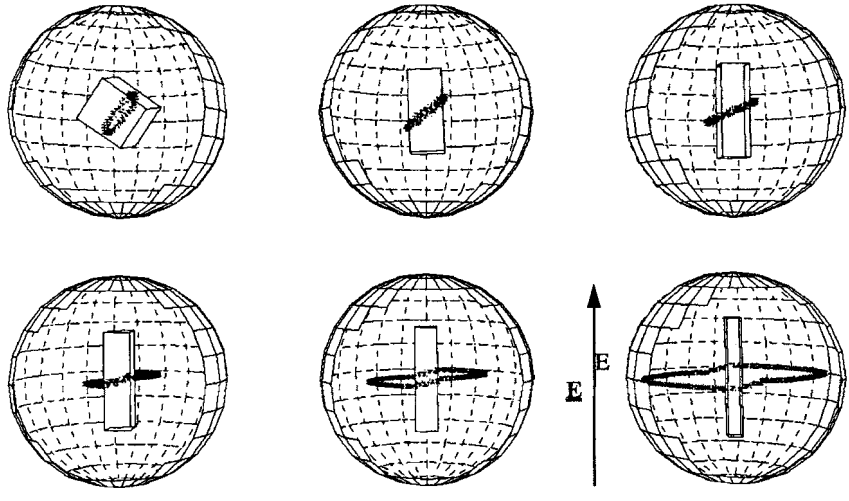

Figure 3. Six stages of the orientation of an axial droplet by an external field.

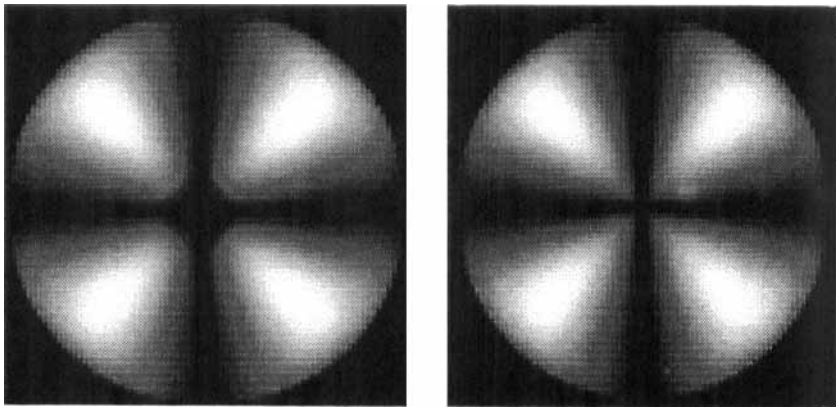

(*a*) (*b*)

Figure 4. Computed phase contrast pictures of (*a*) the axial and (*b*) the radial director configurations of droplets with homeotropic anchoring.

loop which was quite small in this case. Accordingly, the overall orientation was fairly isotropic and thus did not differ much from a radial configuration.

The axial configuration is energetically preferred to the radial one as a consequence of the rigid anchoring (corresponding to an infinite surface energy), which favours the axial configuration. To check the numerical algorithm in this respect, a radial droplet was modelled, and it turned out that its overall anisotropic energy was about 10 times higher than that of the axial one. The radial configuration was of course stable, but it could be transformed to an axial one by the application of an electric field. Figure 4 shows computed phase contrast pictures of a radial and an axial director configuration. The main difference is, that the 'Maltese cross' is well defined in the centre for a radial droplet, whereas the axial droplet is black inside the disclination ring.

Next, an external field of $E \sim 5\ E_{\text{fred}}$ was applied to the previously obtained axial droplet, and $\Delta\varepsilon$ assumed positive (there is no real Freedericks threshold for the radial geometry but rather is E_{fred} a reference value for the dimensionless algorithm). Six stages of the reorientation process are displayed in figure 4: the disclination ring grows and rotates in the direction of the external field, and at the same time increases the weak anisotropy of the overall alignment represented by the rectangular box in the droplet centre. Once oriented in the direction of the external field, the droplet axis, which is defined by the disclination ring rather than by the insignificant equilibrium anisotropy, keeps its position when the field is switched off (not shown).

3.2. *Planar aligned droplets*

Here, the previously mentioned *true planar boundary conditions* were applied. Again, the simple algorithm for a fixed scalar order parameter, with quasi-isotropic initial conditions was used. The relaxation process is depicted in figure 5: first, a network of disclination lines which end at the surface is generated. This simplifies to two lines that shorten to half-loops which are located at antipodal points. In equilibrium, the overall alignment is well defined in the direction of the defects, and uniaxial. This configuration is very similar to the bipolar director configuration, with the only difference that the boojums are represented by short half-loops. This difference is fundamental from a topological point of view, because lines and points are different objects. In practice, however, there is not much difference: if the endpoints of the loop

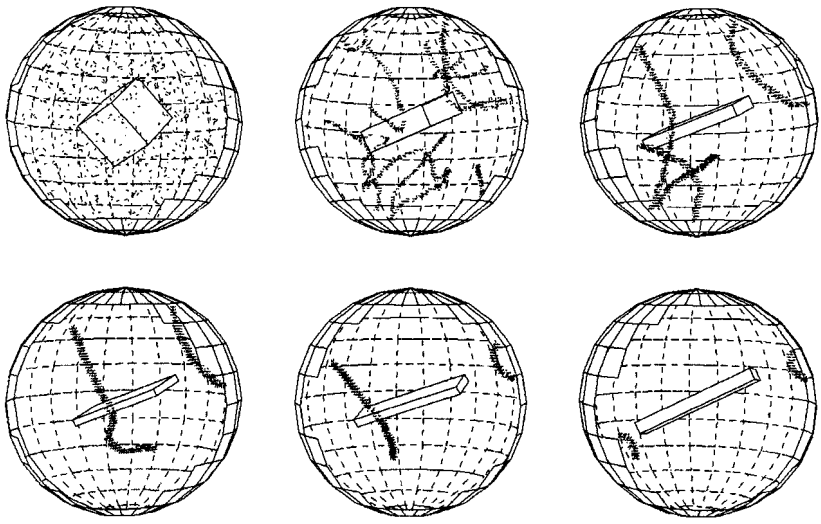

Figure 5. Relaxation of a droplet with planar surface alignment from the quasi-isotropic state; $t/\delta t = 0$, 800, 2000, 3000, 7000 and 31 000.

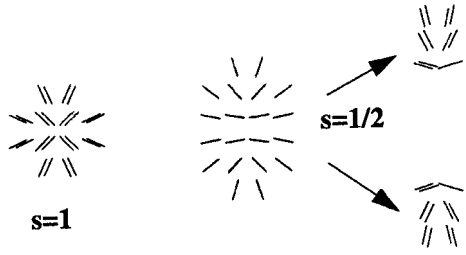

Figure 6. Two surface defects of strength 1/2 can continuously be transformed into one defect of strength 1.

are close enough together the director field becomes indistinguishable from that of a boojum (see figure 6). Thus, the half-loops provide a microscopic model for the surface disclinations of strength 1, which arose without any further assumptions from the true planar boundary conditions.

Next, a two-frequency control of the droplet being considered was simulated. The simulation worked in principle as it should, that is, the droplet axis could be rotated in direction of the applied field, and also perpendicular to the field. During the reorientation the biaxial director configuration was preserved. It should be mentioned that the reorientation was not a smooth process but happened in small steps, as if the director field were stuck to the boundary. This is reflected by the elastic energy of the droplet as a function of time, shown in figure 7. I believe these steps to be an artifact of the discretization; the interesting thing here, however, is that a similar behaviour is known from experiment with very small droplets [12].

3.2.1. *Influence of the cavity anisotropy*

It is known from experiment [1] that the director axis of a bipolar droplet with elongated cavity has a home position which is parallel to the cavity axis. After a

Figure 7. Elastic energy during reorientation of a bipolar droplet by an external field.

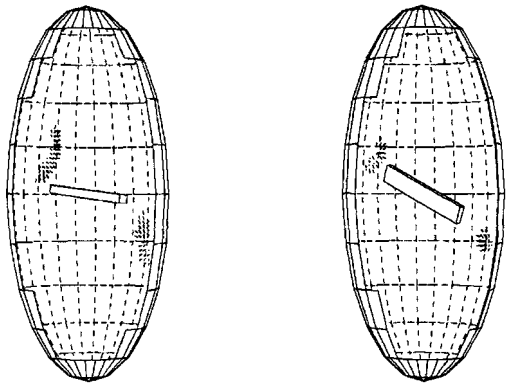

Figure 8. Bipolar droplet with elongated cavity. After reorientation by an electric field (left) the droplet relaxes (right) to a state with a small cavity-induced overall-biaxiality.

reorientation by an external field, it returns into this position. The simulation did not exhibit such behaviour, probably due to the previously mentioned 'sticking'. Instead, it showed a small cavity-induced biaxiality (see figure 8).

3.3. *Heating up planar aligned droplets*

For this simulation, the extended algorithm containing the Landau–De Gennes potential was used. In contrast to the simple algorithm, the length scaling is fixed. I chose a length scaling of $\delta x/\xi_0 = 10$; the corresponding maximum numerically stable time step was $\delta t = \tau_a$. For material parameters like $K = 1{\cdot}3 \times 10^{-11}$ N and $\gamma_1 = 0{\cdot}15$ Pa s (for example MBBA), this corresponds to a droplet diameter of about 0·6 μm and a time step of $\delta t = 17$ ns (see equation (3)).

Again, a quasi-isotropic initial state was chosen, and a temperature $T = T^*$ (the pseudo-critical temperature, below which no metastable isotropic phase can exist). It took the droplet 300 000 time steps = 5 ms to relax to the bipolar configuration. Although the spatial resolution was lower than in the above simulation with the simple algorithm (the droplet diameter was reduced from 80 to 50 grid points), ten times more time steps were needed. Also, the amount of floating point operations needed to

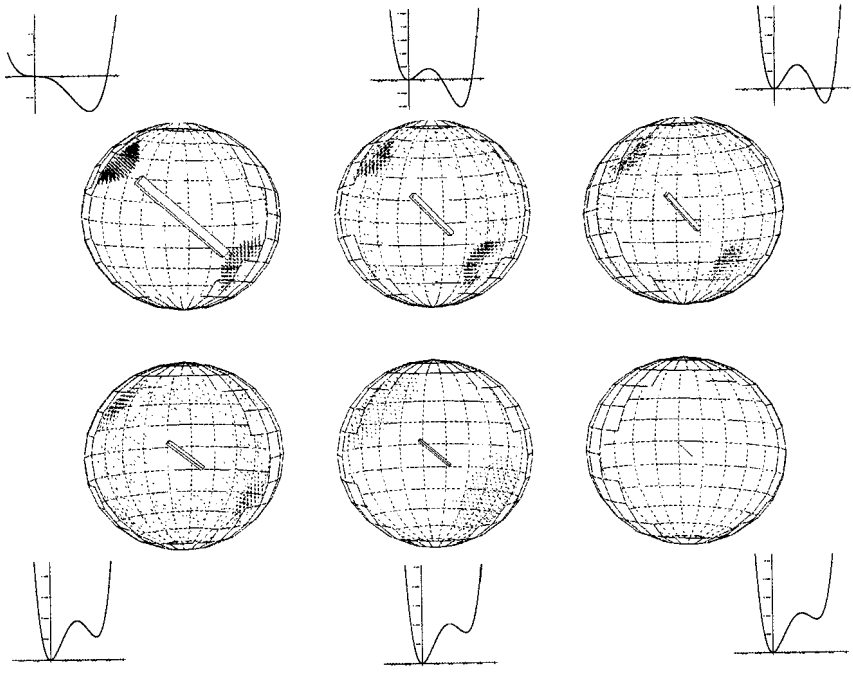

Figure 9. Six stages of heating a bipolar droplet. It seems that the director configuration changes from half-loops to real boojums between the third and the fourth picture.

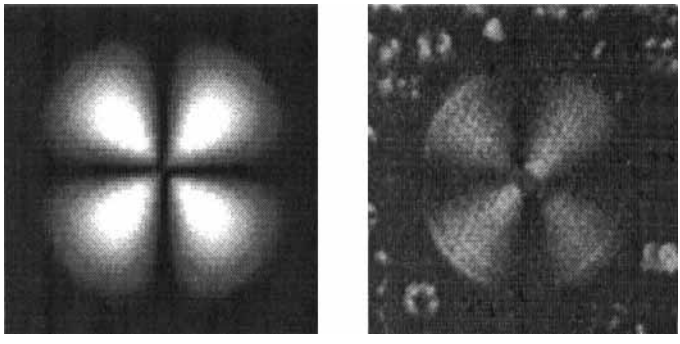

(*a*) (*b*)

Figure 10. (*a*) Computed phase contrast picture of a simulated bipolar droplet with half-loops and (*b*) photograph of a bipolar droplet.

perform one time step was considerably higher. The computing time for this simulation was about 70 hours on a Hewlett–Packard 720 workstation in single user mode. The results of this simulation are comparable to those of the other one and are therefore not presented. Next, the droplet was heated above the clearing point as slowly as possible (with respect to the time consuming algorithm). In figure 9 six stages of the phase transition are displayed. Instead of naming the respective reduced temperatures, I found it more instructive to express the temperatures by their corresponding Landau–De Gennes potentials. The results are: the bipolar configuration is preserved, but the scalar order parameter decreases. So far, not surprising. Unexpected is the change in the director configuration from the half loops to real boojums, which takes place

between the third and the fourth picture, that is, close to the nematic–isotropic transition temperature. Unfortunately, it will be difficult to separate these two configurations in an experiment: a computed phase contrast picture of a bipolar configuration with half-loops looks very similar to a photograph of a real one (see figure 10).

4. Conclusions

The numerical method proved capable of simulating some of the director configurations of nematic droplets. The relaxation from the quasi-isotropic state ensures that the equilibrium configurations found are unbiased by any presuppositions.

On the basis of the correct nematic symmetry and a new type of boundary condition, referred to as true planar anchoring, a 'microscopic' model of the $s=1$ surface disclination points (boojums), that is, disclination half-loops, arose without any additional assumptions.

An enhancement of the algorithm including a variable scalar order parameter leads to the interesting prediction, that the disclination half-loops will transform to real boojums when the probe is heated beyond the clearing point. This prediction, however, can only be checked if short half loops can be distinguished from real boojums experimentally.

The reorientation of bipolar configured droplets by cavity anisotropy failed, which may be a hint that, in this case, material transport is one of the relevant mechanisms.

Financial support of the Deutsche Forchungsgemeinschaft via the Sonderforschungsbereich 'Anisotrope Fluide' is gratefully acknowledged. I thank Professor Dr S. Hess and Dr H. Kitzerow (TU Berlin) for their assistance.

References

[1] DOANE, J. W., GOLEMME, A., WEST, J. L., WHITEHEAD, J. B., and WU, B. G., 1988, *Molec. Crystals liq. Crystals*, **165**, 511; ONDRIS-CRAWFORD, R., BOYKO, E. P., WAGNER, B. G., ERDMANN, J. H., ZUMER, S., and DOANE, J. W., 1991, *J. appl. Phys.*, **69**, 6380.
[2] CROOKER, P. P., and YANG, D. K., 1990, *Appl. Phys. Lett.*, **57**, 2529.
[3] LAVRENTOVICH, O. D., and SERVAN, V. V., 1990, *Nuovo Cim.*, **12**, 1219.
[4] KILIAN, A., and HESS, S., 1989, *Z. Naturf.* (*a*), **44**, 693; 1990, *Liq. Crystals*, **8**, 465.
[5] KILIAN, A., 1992, *Molec. Crystals liq. Crystals Lett.*, **8**, 91.
[6] DRZAIC, P. S., 1988, *Molec. Crystals liq. Crystals*, **154**, 239.
[7] ERDMANN, H., ZUMER, S., and DOANE, J. W., 1990, *Phys. Rev. Lett.*, **64**, 1907.
[8] LAVRENTOVICH, O. D., and TERENT'EV, 1986, *Sov. Phys. JETP.*, **64**, 1237.
[9] HESS, S., and PARDOWITZ, I., 1981, *Z. Naturf.* (*a*), **36**, 554.
[10] KAISER, P., WIESE, W., and HESS, S., 1992, *J. Non-Equilib. Thermodyn.*, **17**, 153.
[11] SHURCLIFF, W. A., 1966, *Polarized Light* (Harvard University Press).
[12] DRZAIC, P. S. (private communication).
[13] CHICCLOLI, C., PASINI, P., SEMERIA, F., and ZANNONI, C., 1990, *Phys. Lett.* A, **150**, 311; 1992, *Molec. Crystals liq. Crystals*, **212**, 197.